PRAMANA
—journal of
physics

© Printed in India

Vol. 49, No. 2,
August 1997
pp. 239–252

Modified WKB transmission for fusion

S V S SASTRY and S K KATARIA
Nuclear Physics Division, Bhabha Atomic Research Centre, Mumbai 400085, India

Abstract. In the optical model (OM) approach for fusion, absorption of flux occuring beyond the barrier position is presented in detail at low energies. It has been shown that the OM transmission can be well approximated as a sum of the WKB transmission and a long range absorption (LRA) contribution. Owing to absence of LRA, the fusion predictions of coupled channel codes based on transmission approach like the CCFUS code, do not agree with the predictions of complete coupled reaction channel (CRC) calculations based on OM approach using the code FRESCO. The CCFUS code with a modified transmission which includes LRA contribution is shown to be consistent with the CRC results using FRESCO. The static deformation of the colliding nuclei strongly influences the fusion imaginary potential and therefore the deep sub-barrier fusion cross sections.

Keywords. Sub-barrier fusion; CRC calculations; barrier penetration; WKB transmission; optical model; long ranged absorption; deformed potentials.

PACS Nos 25.70; 24.10

1. Introduction

The study of heavy ion (HI) reactions over the past decade has yielded lot of information about the reaction mechanism and the inter-relation between various reaction channels. The coupled channels (CC, also denoted by CRC) formalism is very successful in explaining most of the experimental data of HI fusion around the barrier energies and also the channel coupling effects on elastic and various other reaction channels [1,2]. HI fusion, as described by the CC formalism, is estimated as the flux that is absorbed from the coupled channels system by using a short ranged imaginary potential [3,4] (FRESCO code [3]). Alternatively, fusion is also obtained by means of ingoing wave boundary condition in each channel for the flux that traverses the barrier. This barrier tunnelling flux is obtained by using WKB method for transmission through the real barrier. At present there are very few reported coupled reaction channel (CRC) calculations using comprehensive coupling scheme like the case reported in ref. [4]. However, complete CRC calculations for many HI systems especially with deformed targets like ^{232}Th are very difficult as couplings to several inelastic and transfer channels can contribute significantly to fusion enhancement. For example, even for the case of spherical system of $^{16}O+^{208}Pb$ (see ref. [4]) inclusion of α transfer channel is important for fusion, despite the inclusion of several channels for inelastic excitations, neutron and proton transfers to respective ground states and a few excited states. Therefore, these calculations are sometimes not feasible owing to the need of enormous computation time and memory. In such cases one often uses simplifed CC codes like CCFUS for a quick and approximate

estimation of coupling effects [5] (only on fusion channel). The code CCFUS uses the Hill–Wheeler transmission formula in addition to various approximations used to diagonalize the coupled equations [5]. These approximations greatly simplify the coupled channel problem and thus reduce the computation time and memory requirements, though at the cost of loosing information about other channels. Consequently, this code has been successfully used to understand the experimental fusion data for various HI systems around the barrier energies.

However, the recent extensive study of the sub-barrier fusion cross section at low energies and the experimental measurements of fusion mean square spin [FMSS, cf. eq. (1a)] by various methods have led to new results that are not in agreement with the current model predictions [1, 2]. These results can be summarized as (i) the anomalous enhancement of FMSS as derived from the fission angular anisotropy measurements and (ii) the anomalous enhancement of fusion cross section at deep sub-barrier energies [6]. The CCFUS code fails to qualitatively explain these anomalous results. It was first demonstrated by Satchler *et al* that a long ranged optical potential for fusion can explain the anomalous FMSS values [7]. In this method, the flux is absorbed at large distances in contrast to the requirement of complete traversal of barrier of the transmission approach. Thus it is necessary to examine these approaches for fusion in detail. It is generally believed that the barrier penetration model and the optical model absorption with short ranged imaginary potential ($r_i = 1.0$ fm) give similar results for fusion spin distributions [8]. However, it was shown for HI systems at deep sub-barrier energies, the WKB transmission method underpredicts the FMSS of an OM calculation [9]. As a result, the predictions of coupled channel codes based on WKB transmission formula (for example CCFUS) will not be in agreement with FRESCO calculations at very low energies as reported in ref. [9]. In § 2, we present the radial distribution flux of OM absorption at different energies and a simple correction to barrier transmission formula consistent with OM absorption of flux. In § 3, a simple procedure will be presented to incorporate the long range absorption (LRA) effects in the barrier transmission formula in the presence of couplings. In § 4, the present work will be applied to analyse the deep sub-barrier fusion of some recently reported heavy ion systems. In §5, we present the OM absorption for the systems with static deformation and in § 6, a brief summary.

2. OM and WKB transmissions for fusion

As mentioned earlier, it is generally believed that the results of barrier penetration model agree with the optical model absorption using short ranged imaginary potentials. On the contrary, we showed for HI systems that these approaches strongly disagree at low energies. At above barrier energies for heavy ion systems, these approaches give similar results owing to the fact that the transmission is nearly unity. However, there is a misconception that the discrepancy shown for heavy ion case is valid for light ion case as well. Therefore in the following, we present the results for OM absorption of flux by imaginary potentials and compare with the results of transmission method. Figure 1 shows the fusion excitation function for the light ion case of $p+^{238}$U and the parameters of OM potentials of volume Woods–Saxon type are: $r_c = 1.3$ fm, $V_0 = 50$ MeV, $r_0 = r_i = 1.355$ fm, $a_0 = a_i = 0.635$ fm, $W_0 = 5$ MeV. It can be seen from the figure

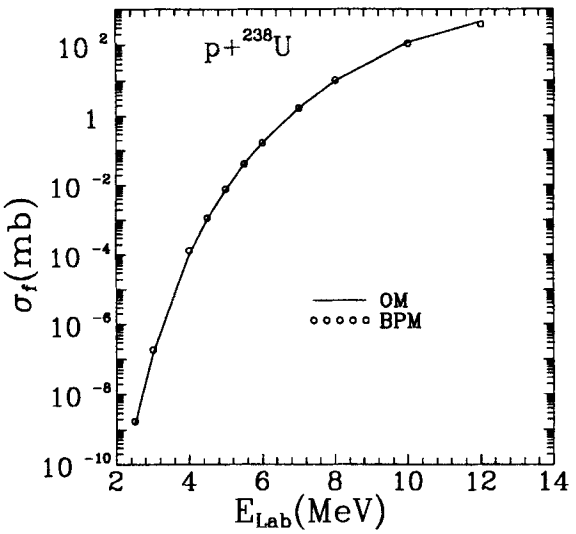

Figure 1. Comparison of the OM absorption excitation function and the fusion excitation function from transmission method for the case of $p + {}^{238}\mathrm{U}$. The solid curve represents OM results and the circles represent the transmission model results.

that the OM absorption cross sections agree well with the results of WKB transmission of flux through the corresponding real barrier. This agreement of results down to deep sub-barrier energy of 2 MeV of proton has been observed in spite of use of large r.m.s. radius ($r_i = 1.355$) and large diffuseness (0.635 fm) for this system in contrast to the findings for a heavy ion case shown in ref. [9]. This happens because at low energies the corresponding R_m values [cf. eq. (4)] for light ion case, where the LRA is maximum, turns out to be very large. Therefore, the LRA effect is insignificant for the light ion case as the $W(r)$ in this region is extremely small, unlike the case for heavy ions.

In the following, we present the results for heavy ion system of ${}^{16}\mathrm{O} + {}^{208}\mathrm{Pb}$. The absorption of flux in the OM depends on the choice of imaginary potential and therefore extends over the entire domain of the radial integration. The OM radial distribution of flux absorbed ($A_l(r)$) and the cross section (σ_l) are related by

$$\sigma_l = \int_0^\infty A_l(r)\mathrm{d}r = \frac{-8}{\hbar v}\frac{\pi}{k^2}(2l+1)\int_0^\infty |u_l(r)|^2 W(r)\mathrm{d}r \tag{1}$$

and the FMSS (in units of $\hbar^2$) by

$$\langle L^2\rangle = \sum l^2\sigma_l / \sum \sigma_l . \tag{1a}$$

Here, $|u_l(r)|^2$ is the radial density of the wave function for partial wave l. Figure 2(a) shows the radial density distribution versus radial separation for different partial waves at 72 MeV lab energy along with the imaginary potential, $W(r)$. It can be seen from the figure that the cross section is determined by overlap of imaginary potential (W) which decreases exponentially and the radial density distribution of the wave function that increases with radial separation. As seen in figure 2(b), this overlap integral has

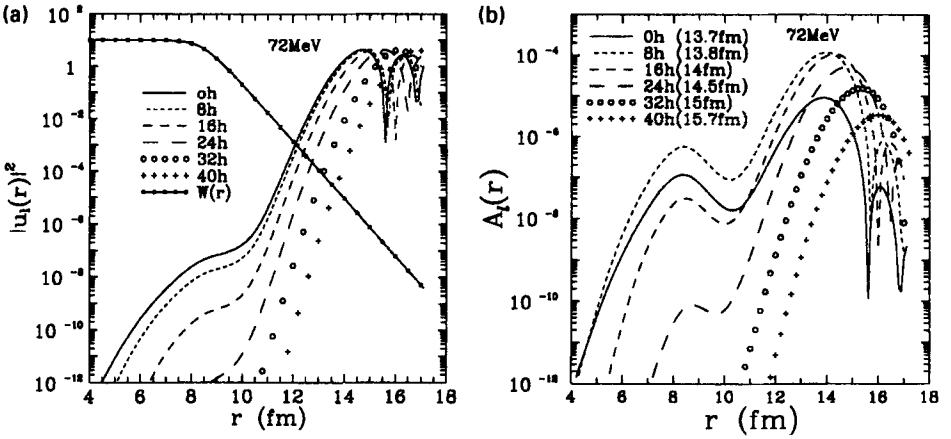

Figure 2. (a) Radial density of the wave function, $|u_l(r)|^2$ versus r at 72 MeV lab energy for different partial waves as labelled in the figure. The imaginary potential, $W(r)$, is shown by dashed curve. The OM code SNOOPY is used with OM potential (Woods–Saxon form) parameters as follows: $r_c = 1.23$ fm, $V_0 = 60.5$ MeV $r_0 = 1.179$ fm, $a_0 = 0.685$ fm, $W = 10$ MeV, $r_i = 1.0$ fm, $a_i = 0.40$ fm. (**b**). Radial distribution of absorption of flux ($A_l(r)$) in OM corresponding to figure 2(a) for different partial waves shown by different symbols. The R_m values for different l values obtained from eq. (4) are indicated in parentheses.

significant contribution beyond the barrier position at very low energies depending on $W(r)$ and the l value. The wave function exhibits strong oscillations at large distances which are weighted by the $W(r)$. Therefore, $A_l(r)$ exhibits multiple peaks and the lowest one is around the barrier position ($R_b = 11$ fm) as used in the standard barrier transmission models. The next significant peak in $A_l(r)$ occurs around the classical turning point (R_0) and corresponds to absorption beyond the barrier position. This becomes obvious when eq. (1) is written as

$$\sigma_l = \frac{-8}{\hbar v}\frac{\pi}{k^2}(2l+1)\left[\int_0^{R_b} |u_l(r)|^2 W(r)\mathrm{d}r + \int_{R_b}^{\infty} |u_l(r)|^2 W(r)\mathrm{d}r\right] \tag{2a}$$

$$= \sigma_l^{(1)} + \sigma_l^{\mathrm{LRA}}. \tag{2b}$$

$\sigma_l^{(1)}$ can be approximated by the WKB transmission of flux through the real barrier, provided the imaginary strength W_0, is not vanishingly small. The OM transmission of flux is nearly independent of this parameter for small values of W_0 [8]. Therefore, the first part of eq. (2a) can be written as

$$\sigma_l^{(1)} \approx \frac{\pi}{k^2}(2l+1)T_l^{\mathrm{WKB}}. \tag{2c}$$

The second part, σ_l^{LRA} represents the long range absorption (LRA). At deep sub-barrier energies and in WKB approximation, the raidal wave function can be written as [10]

$$u_l(r) \approx \mathrm{e}^{\int_{R0}^{r} k(r')\mathrm{d}r'} \quad \text{for } r < R_0 \tag{3a}$$

with $k(r) = k((2\eta/kr) + (L^2/k^2r^2) - 1)^{1/2}$, η is the Sommerfeld parameter and k is the incident wave number. For radial separations beyond $R_0, u_l(r)$ is taken to be unity. Though this is overestimation of the flux at large distances, it is a good approximation. Under these approximations, the second part of eq. (2a) can also be written as

$$\sigma_l^{\mathrm{LRA}} = -C_l \int_{R_b}^{\infty} \mathrm{d}r \exp\left(-\kappa r + 2\int_{R_0}^{r} k(r')\,\mathrm{d}r'\right) \tag{3b}$$

with

$$C_l = 10(2l+1)\pi/k^2 8/\hbar v W_0 \mathrm{e}^{\kappa r_i} \tag{3c}$$

and $k(r')$ is the local wave number in the presence of Coulomb and centrifugal potentials and $\kappa = 1/a_i$ is the inverse of diffuseness of the fusion imaginary potential $W(r)$ in

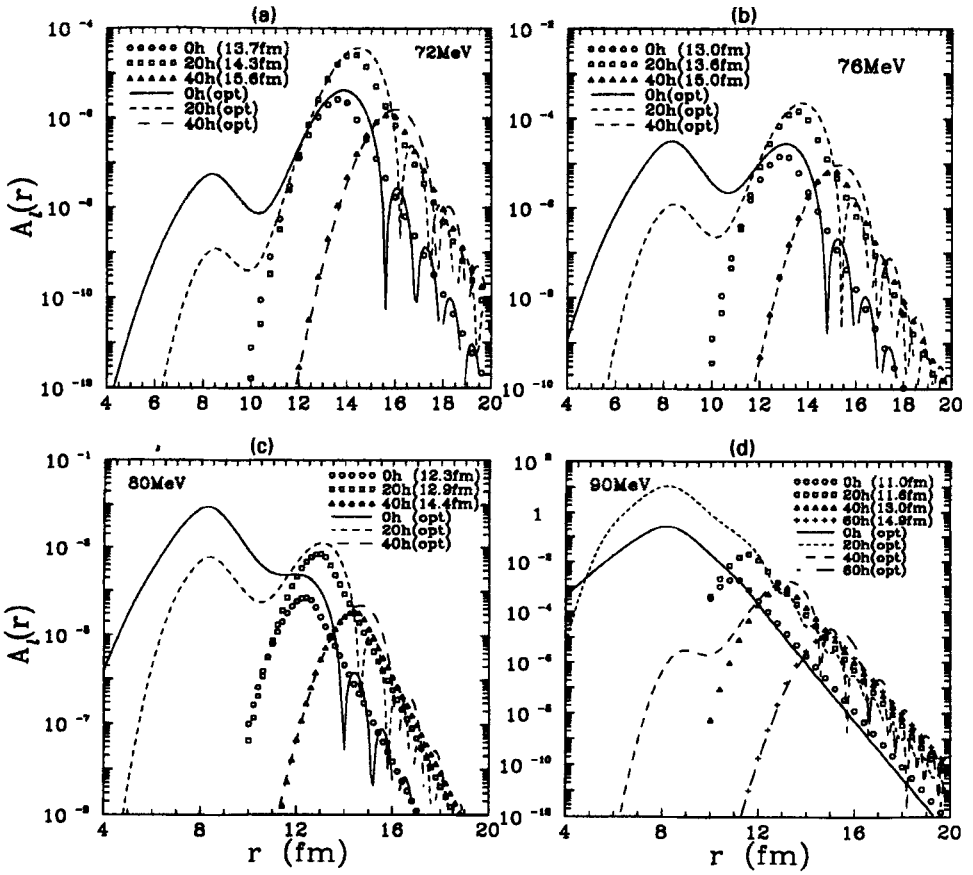

Figure 3(a, b, c, d). Comparision of radial distribution of flux at large distances for OM and WKB integrand of eq. (3b). Here, **(a)** is for 72 MeV, **(b)** for 76 MeV and **(c)** for 80 MeV and **(d)** for 90 MeV lab energies. As shown in these figures, the continuous curves for various partial waves represent OM results obtained from the OM code SNOOPY. The symbols represent the WKB results of eq. (3b) for different partial waves. The R_m values for different L values obtained from eq. (4) are shown in parentheses. The OM potential parameters are the same as in figure 2.

eq. (1). Following the procedure of ref. [10] (similar integrals for particle transfer) the distance, R_m, where the LRA contribution is maximum can be obtained from [9]

$$R_m = \frac{\eta}{kq^2}\left(1+\left(1+\frac{q^2L^2}{\eta^2}\right)^{1/2}\right) \quad \text{and} \quad q^2 = 1+\kappa^2/4k^2. \tag{4}$$

The integrand of eq. (3b) can be approximated as a gaussian centered around R_m as in ref. [10]

$$\sigma_l^{\mathrm{LRA}} = 2C_l \int_{R_0}^{R_m} \mathrm{d}r \exp\left(-\kappa r + 2\int_{R_0}^{r} k(r')\mathrm{d}r'\right). \tag{5}$$

One can also use eq. (3b) replacing R_b and ∞ of outermost integral with some suitable limits beyond the barrier position. In the present work, we used eq. (3b) and the limits taken are 12 fm and 20 fm respectively. Further, for integration along a Coulomb trajectory, the integrand of eq. (3a) and also the corresponding terms in eq. (3b) were replaced by an analytic expression.

This integrand of eq. (3b) (alongwith multiplicative factor $-C_l$) is shown by various symbols in figures 3(a, b, c, d). As seen in figures, this approximation agrees well with the $A_l(r)$ obtained from OM code, represented by various continuous curves. The R_m values represented by eq. (4) for different partial waves are indicated in parentheses in figure 2(b) and also in figures 3(a, b, c, d). As seen in figure, at high energies the lowest peak around R_b only contributes. This is the usual WKB transmission of flux through the fusion barrier and is independent of W_0 as represented by the first term of eq. (2b). It is at low energies that the second term of eq. (2b) contributes significantly, which contains the LRA effects of the OM approach and is responsible for large OM estimates of FMSS. It is obvious that if the second term is neglected, the OM also predicts saturation values for FMSS like the WKB method. Thus the LRA effects will be seen in any CRC code which uses OM approach for fusion.

3. Coupled channels method for fusion

In the CC formalism, there are several channels from which absorption takes place but, applying eq. (3b) to all the channels in order to obtain LRA contribution may not be really necessary. In order to use the approximations of the preceeding section, it is necessary to understand how absorption of flux takes place from various channels of a coupled system. The CRC calculations for $^{16}O+^{208}Pb$ system were performed using the code FRESCO coupling to four inelastic channels [4, 9] (five channels including elastic channel). In the CRC formalism, fusion is given by (cf. eq. A2 of [11]),

$$\sigma_f = \sum_{\alpha\beta} \frac{-2}{\hbar v} \langle \chi_\alpha^+(k_\alpha)|W_{\alpha\beta}|\chi_\beta^+(k_\beta)\rangle, \tag{6a}$$

$$\chi_\alpha^+(k_\alpha, r) = \frac{1}{kr}\sum_l (2l+1) i^l \chi_{\alpha,l}(k,r) p_l(\hat{k}.\hat{r}), \tag{6b}$$

$$\sigma_f = \sum_{\alpha\beta} \frac{-8}{\hbar v}\frac{\pi}{k^2}\sum_l (2l+1)\langle \chi_{\alpha,l}|W_{\alpha,\beta}|\chi_{\beta,l}\rangle, \tag{6c}$$

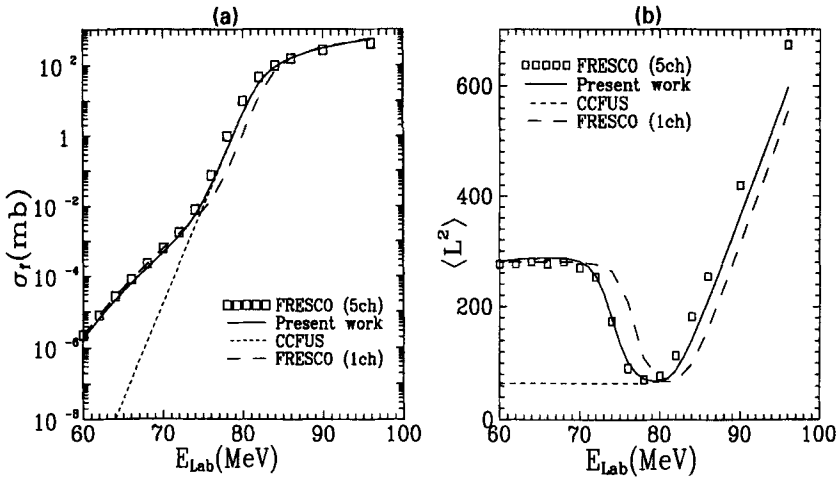

Figure 4. (**a**) Comparison of CRC results and the results of modified CCFUS code. As labelled in the figure, the CRC fusion (absorption) excitation function obtained from FRESCO is represented by squares. The results from CCFUS with modified transmission formula is shown by a solid curve along with the CCFUS results using WKB transmission formula for fusion (short dashed curve). The long dashes indicate the fusion predictions of FRESCO with only elastic channel. (**b**) FMSS versus energy for various cases of figure 4(a). This is to compare the modified CCFUS results with CRC calculations.

where α and β are the various channels included in the CRC calculations and $\chi_\alpha^+(k_\alpha)$ is the outgoing wave function for relative motion of coupled equations in channel α.

It should be noted that the term fusion here refers to removal of flux by OM imaginary potentials from the coupled channels system. Therefore, the fusion excitation function in these calculations refers to absorption excitation function. The fusion excitation function by the CRC method for different a_i values was studied using eq. (6). It was seen that as long as the fusion potential is very short ranged, the OM approach for fusion gives the same results as WKB transmission method. Thus, the diffuseness parameter of fusion imaginary potential serves as a measure of LRA for fusion in OM approach. The CRC fusion excitation function differs from the corresponding uncoupled case around the barrier energies depending on a_i value and merges with it at deep sub-barrier energies (LRA effect). For example, see the squares and long dashed curve in figure 4(a). The corresponding CRC results for FMSS at low energies show an increasing trend depending on a_i. As an example, figure 4(b) shows the CRC results using FRESCO for FMSS with $a_i = 0.8$ fm (Woods–Saxon square form) represented by squares. The FMSS for coupled cases (squares) for a given a_i was also observed to merge with the corresponding uncoupled case (long dashes) at very low energies owing to LRA effect (for more details see ref. [9]). One can therefore conclude that the absorption into the fusion channel at deep sub barrier energies takes place predominantly from the coupled elastic channel alone and in comparison the absorption from the other channels is negligible. In orther words, at very low energy it suffices to use only elastic channel for calculating LRA contribution instead of the summation over all the channels in eq. (6).

As discussed earlier, the CCFUS code based on WKB transmission formula will not be equivalent to complete CRC calculations using the codes like ECIS and FRESCO. Figure 4(a) shows the fusion excitation function obtained from FRESCO code (squares) and from the CCFUS code with WKB transmission approach (short dashed curve). The anomalous enhancement of the CRC results (squares) compared to CCFUS (short dashed curves) results is owing to LRA effect. Figure 4(b) shows the corresponding FMSS results. In order to remove this defficiency, the WKB transmission in CCFUS has been modified by using only elastic channel represented by $\sigma_l^{(m)}$,

$$\sigma_l^{(m)} = \frac{\pi}{k^2}(2l+1)\,T_l^{\mathrm{CC}} + \sigma_l^{\mathrm{LRA}}. \tag{6d}$$

Here, T_l^{CC} is the transmission for fusion from usual unmodified CCFUS code which includes all the effects of channel couplings. The second term σ_l^{LRA} is same as in eq. (3b). In addition, the WKB radial wave function part in eq. (3b) was replaced by analytical expression for a Coulomb trajectory. Under these conditions, the integral of eq. (3b) can be seen to be very simple and is evaluated once for each partial wave, irrespective of the number of channels coupled. Therefore, the computation time and memory requirements are almost unchanged.

Figure 4(a) also shows the fusion excitation function by the modified CCFUS method using eq. (6d) (solid curve), FRESCO (squares) and the unmodified CCFUS results (short dashes) for a_i value of 0.4 fm (equivalent to 0.8 fm in FRESCO with W-S square form). The W_0 used is 10 MeV and r_i is 1.0 fm which are same as CRC input. Figure 4(b) shows the corresponding FMSS values. As shown in figure 4(a,b), the results of modified CCFUS code compare well with CRC results using FRESCO. The good agreement between these two cases means that the proposed modification is a good approximation for simulating the results of realistic CRC codes. Therefore, this modification can be used for parametrizing the experimental data on heavy ion fusion.

4. Deep sub-barrier fusion of heavy ion systems

Using the modified CCFUS code, we have calculated the fusion of (^{11}B,^{19}F,^{28}Si)+^{232}Th systems. The imaginary potential parameters used in CCFUS are $r_i = 1.0$ fm, $W_0 = 10$ MeV and a_i is taken to be 0.55 fm. The deformation parameters used for ^{232}Th are $\beta_2 = 0.22$ and $\beta_4 = 0.09$. With these parameters, the fusion cross-sections and the FMSS values for these systems obtained from CCFUS are shown by solid curves in figure 5(a, b). The experimental cross section data for these systems [6] also shows similar features as shown in figure 5(a). However, the unmodified CCFUS will not be able to account for this anomalous cross section enhancement of excitation function at deep sub-barrier energies. As shown in figure 5(b), the fusion $\langle L^2 \rangle$ values show increasing trend at deep sub-barrier energies due to LRA effects whereas the channel coupling effects are dominant only around the barrier energies. This enhancement at low energies becomes higher for heavier systems owing to large values of reduced mass and barrier radius and smaller R_m values. This is seen by comparing the results for ^{11}B and ^{28}Si cases in figure 5(b). Therefore, if the LRA effects are incorporated, fusion models give rise to cross section enhancement at deep sub barrier energies in addition to large FMSS.

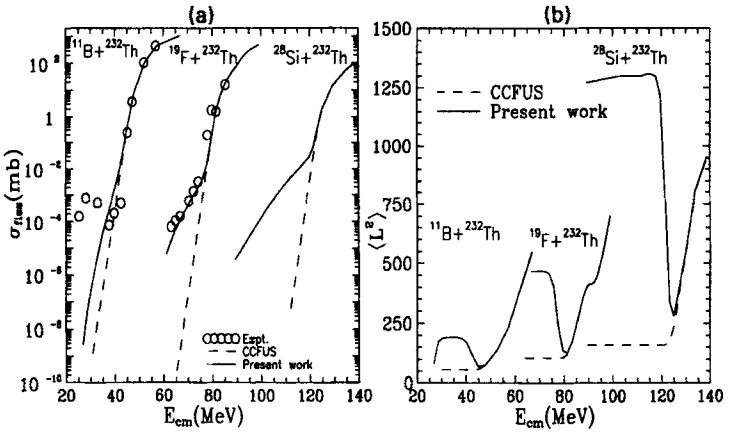

Figure 5. (a) Comparison of the deep sub-barrier fusion predictions of the present method for different systems with same target. The results from CCFUS with modified transmission formula are shown in solid curve along with the CCFUS results using WKB transmission formula for fusion (dashed curve). (b) FMSS versus energy for various cases of figure 5(a). This is to compare the results of CCFUS code using modified and WKB transmission formulae.

It should be noted that the imaginary potential parameters are likely to vary when a comprehensive coupling scheme with all significantly contributing channels is considered for CC calculations. Consequently, the enhancements in excitation function and mean square spin arising due to LRA effects, which depend on imaginary potential, would also change. Therefore, only the qualitative behaviour of the model predictions is of importance. In addition, it should be noted that the entire enhacement observed in deep sub-barrier fusion cross section has been attributed to the LRA effects alone, resulting from spherical imaginary potentials. Consequently, the mean square spin values predicted would provide an upper limit to the fusion $\langle L^2 \rangle$ values for these systems. The effect of static deformation of the potentials on the LRA needs to be investigated and will be discussed in the next section.

5. Absorption in the presence of deformed potentials

So far, the calculations have been based on spherical potentials. When colliding nuclei are statically deformed, one usually incorporates the deformation effects on fusion by averaging the transmission over all orientations of the target, as in the Wong's model for fusion. Similarly, in the OM approach, this static deformation effects must be taken into account for absorption through deformed imaginary potential. Just as the effective real potential is known to become long ranged with large effective diffuseness owing to deformation effect, the short ranged imaginary potential also gets modified. We have introduced the deformation dependence in W by defining the effective imaginary potential averaged over all orientations (θ) of target (considered here is the case of only target deformation). This is similar to the

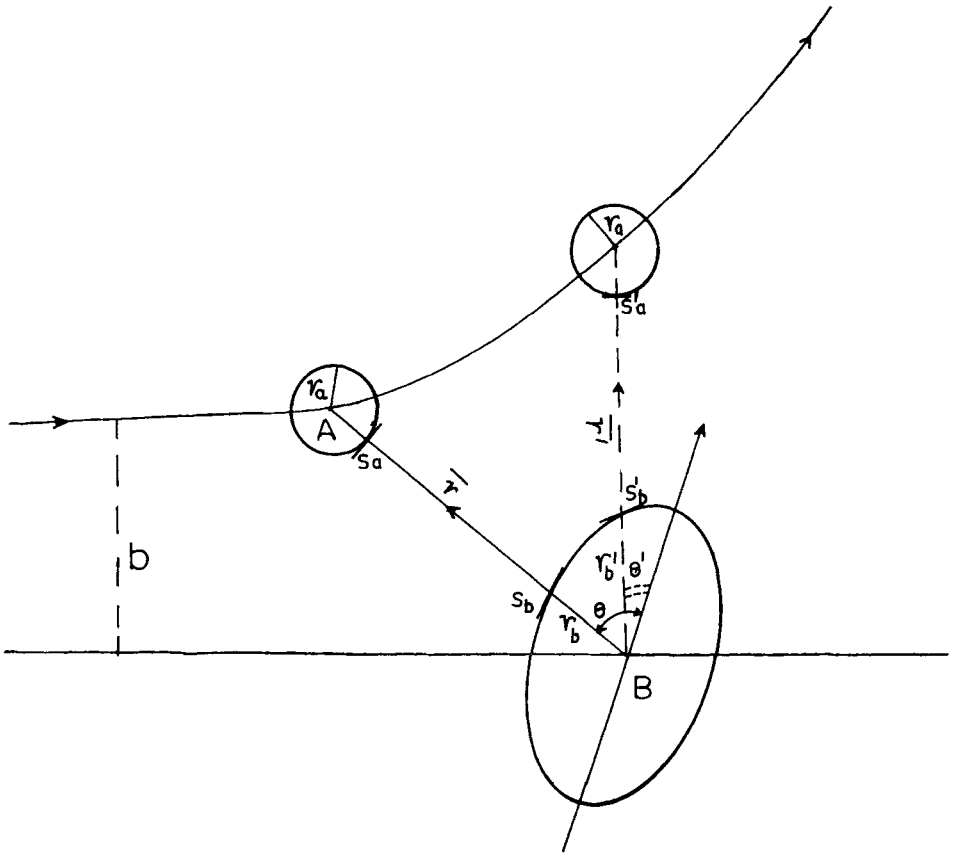

Figure 6. Scattering of spherical projectile from a deformed target of quadrupole deformation, in a semiclassical picture. Here, b is the impact parameter, r_a is the projectile radius, r and r' are the center to center distances between the ions at the positions P and Q along the trajectory. r_b and r'_b are the radii of the deformed target as seen by the projectile at P and Q respectively. The deformation dependent imaginary potential uses the surface to surface distances along the radial direction at P and Q which are given by $r - ra - r_b$ and $r' - ra - r'_b$, of eq. (8)

procedure used in the Wong's model for estimation of fusion as given by

$$\beta_2^b = \frac{\beta_2}{2}\sqrt{\frac{5}{4\pi}}(3\cos^2\theta - 1), \tag{7a}$$

$$\beta_4^b = \frac{\beta_4}{8}\sqrt{\frac{9}{4\pi}}(35\cos^4\theta - 30\cos^2\theta + 3), \tag{7b}$$

$$r_0(\theta) = r_{ab} + r_b(\beta_2^b + \beta_4^b), \tag{7c}$$

with $r_{ab} = r_a + r_b$ and r_a, r_b are the radii of projectile and target respectively, $r_0(\theta)$ is the orientation dependent half radius. The imaginary potential at any relative separation r

between centers of the nuclei is given by

$$W(r,\theta) = \frac{-W_0}{1+\exp((r-r_0(\theta))/a_0)}. \tag{8}$$

The orientation dependence of the potential half radius of eq. (7c) is as shown in figure 6, for the case of scattering from the deformed target with only quadrupole deformation. r_b and r'_b are the radii of the deformed target as seen by the projectile at P and Q along the trajectory. The deformation dependent imaginary potential uses the surface to surface distances along the radial direction at P and Q which are given by $r - ra - r_b$ and $r' - ra - r'_b$, of eq. (8)

Figure 7(a), having four figure sets, shows the effective W as a function of r for different deformation parameter values. Each of these four figures shows the deformation effects for various diffuseness values of the potential. All the potentials used here are of volume Woods–Saxon type and the spherical potential radius parameter is chosen as 1.2 fm. As can be seen from the figure, the effective potential behaves like a potential of larger diffuseness parameter in the neighbourhood of the mean radius. At large distances, it decreases with the same diffuseness as that of the spherical potential. This deformation

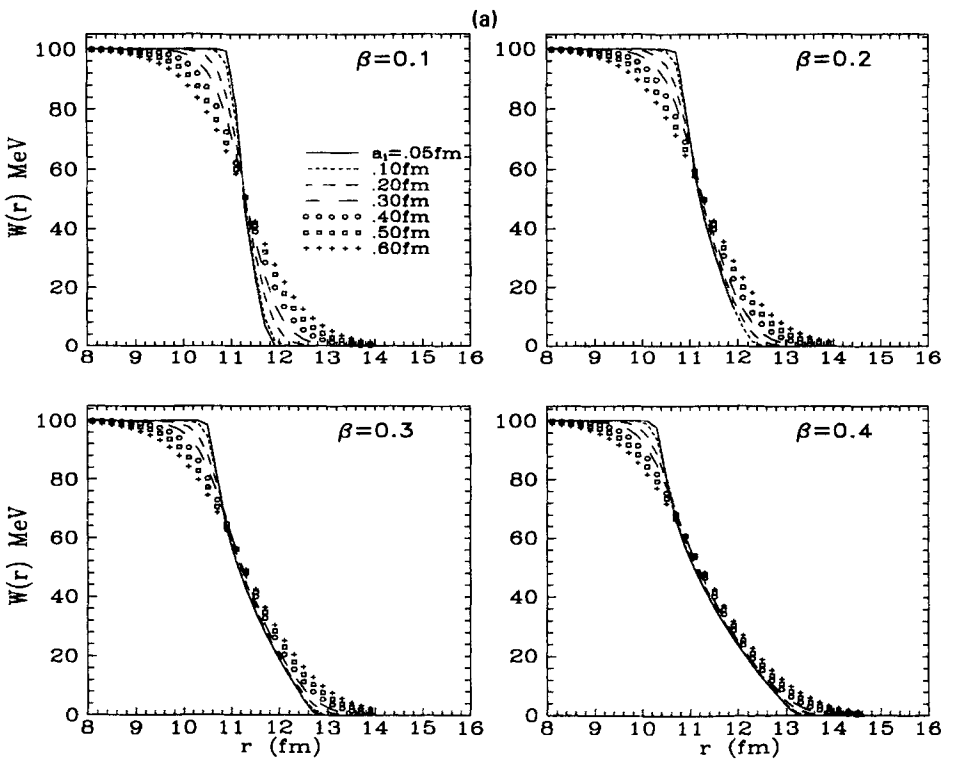

Figure 7(a). Effective W as a function of r for different deformation parameter values (with four figures). Each of these four figures is for different diffuseness values of the spherical potential (i.e. before deformation is switched on), as mentioned in the figure. The spherical potential radius parameter is chosen as 1.2 fm.

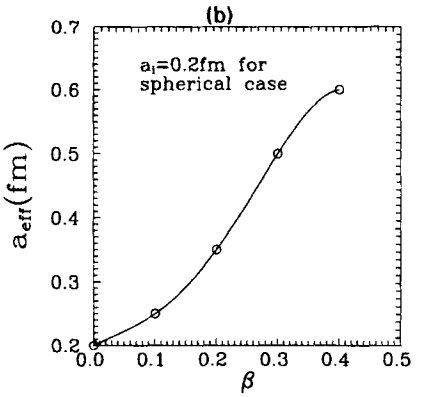

Figure 7(b). Effective diffuseness as a function of deformation (β). The spherical radius parameter is chosen as 1.2 fm.

effect is more pronounced for potentials of smaller diffuseness and only marginal for the potentials of very large diffuseness. For the curve with 0.2 diffuseness and 0.3 deformation parameter values, the effective spherical Woods–Saxon potential that fits in the region of 11 fm to 13.5 fm has a diffuseness of 0.5 fm. Figure 7(b) shows the deformation dependence of effective diffuseness of a Woods–Saxon form that fits the region of 11 fm to 14 fm, which has 0.2 fm diffuseness for corresponding spherical potential. This is the case for which the deformation effect is seen to be maximum. Thus the effect of deformation is that the diffuseness parameter changes from 0.2 fm (i.e. before deformation is switched on) to an effective value of 0.5 fm. In addition, it appears from the figure that the curves representing the different cases of $\{\beta_i, a_j\}$ and $\{\beta_j, a_i\}$ are similar in magnitude. Therefore, the effective potential depends on the combination of both deformation and spherical diffuseness. Since, the fusion imaginary potentials of OM approach are of shorter range and smaller diffuseness, the deformation effect is likely to extend the imaginary potential beyond the barrier radius even though the undeformed potential is very short ranged. Consequently, this effect can result in significant absorption of flux for higher partial waves and therefore results in larger estimates of fusion mean square spin.

Therefore, the CCFUS code has been further modified to incorporate the LRA part of the absorption for each orientation. The orientation dependence is incorporated in W by expanding its mean radius up to quadrupole terms as given by eqs (7, 8). The resultant LRA contribution to transmission is estimated by summing over all the orientations before adding to the coupled channel transmission from usual CCFUS. The results for a test case of $^{19}F + ^{232}Th$ are shown in figure 8 with deformation parameters for Th $\beta_2 = 0.3, \beta_4 = 0.1$ and imaginary potential parameters are $a_i = 0.3$ fm, $r_0 = 1.0$ fm. This leads to three possible cases. The first case is the Wong's model results, corresponding to barrier transmission determined by deformed real potentials (no LRA effects). This is represented by solid curve labelled CC in figure 8. This nomenclature CC has been used instead of Wong because CC here means the usual CCFUS code results which uses Wong's method for transmission in the presence of deformation. The second case is the absorption with LRA contribution for spherical

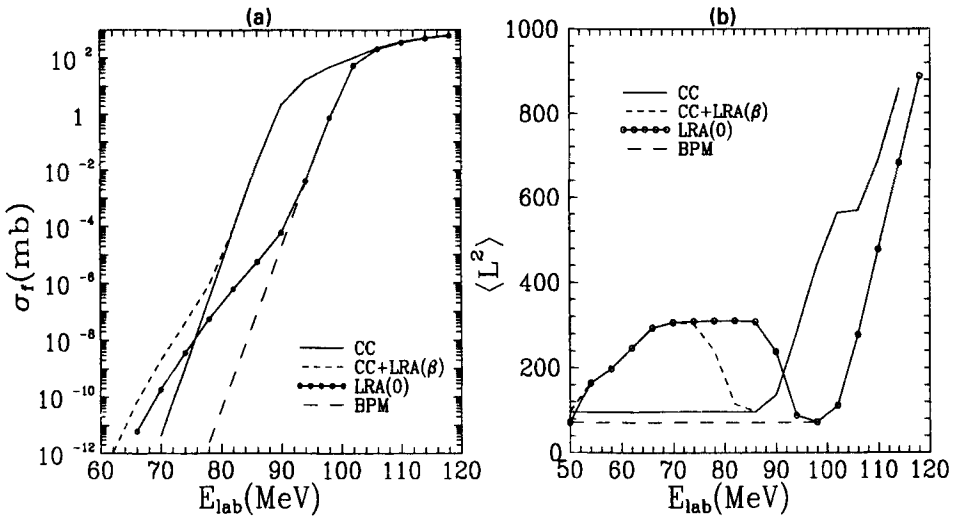

Figure 8(a, b). Effect of deformation of W on LRA contribution, for $^{19}F + ^{232}Th$ system. Figure 8(a) represents the excitation function and figure 8(b) the corresponding mean square spin values. The parameters are $\beta_2 = 0.3$, $r_0 = 1.0$ fm and diffuseness is 0.3 fm. The long dashed curve represents the one dimensional barrier penetration model results. The solid curve labelled CC is the usual CCFUS code results that uses Wong's method in the presence of static deformation. The open squares (interpolated by solid curve) represent the OM and LRA effects, but without deformation of imaginary potential. The short dashed curve represents the OM absorption with LRA in the presence of deformed imaginary potential.

imaginary potential i.e. without deformation effects in W, as represented by open squares interpolated by solid curve. This is equivalent to simple optical model calculation with spherical imaginary potential. The third case is for absorption including LRA in the presence of deformation of W as shown by short dashes. Comparison of these cases shows that the minimum in the FMSS value shifts to lower energies (see short dashes compared to squares) and the peak value of the FMSS enhacement at sub-barrier energies remains the same. At very low energies, these results merge with the corresponding results for the undeformed case.

Therefore, the channel coupling effects are important near the barrier energies, whereas the LRA effects of OM approach are significant only at deep sub-barrier energies. Further, the LRA effects are shifted to lower energies in the presence of static deformation of the imaginary potential. In another study, we have observed that the nonlocal nature of heavy ion potentials also gives fusion cross section enhancement at deep sub-barrier energies. The nonlocal effects result in a higher saturation value for the FMSS compared to usual CCFUS calculations based on local potentials [12]. These nonlocal effects complement the LRA contribution of OM approach for fusion. Thus, the nonlocal and deformation effects should be incorporated in complete CRC codes like ECIS and FRESCO. However, it is not always feasible to perform the comprehensive CRC calculations owing to computation time and memory requirements to analyse the experimental data. The modified CCFUS code has the channel coupling effects, the

optical model LRA effects, deformation dependence of imaginary potentials and further inclusion of nonlocal effects is being studied [12].

6. Summary

It is shown that in the OM, absorption beyond the barrier position is the dominant contribution to fusion at very low energies. This OM results can be expressed as a sum of WKB transmission and an LRA part estimated using WKB elastic wave function. The CRC calculations show that the absorption (mainly LRA) into fusion from elastic channel is the dominant contribution at deep sub-barrier energies. The results of the CCFUS code based on transmission approach, which is very commonly used for fusion calculations, are not in agreement with the CRC results at low energies. The WKB transmission for fusion in CCFUS code has been modified incorporating the LRA term to obtain agreement with FRESCO code, without much additional computation time and memory requirements. The static deformation effect on the short ranged imaginary potentials has been studied using the effective potential as a sum over all the orientations. The effective potential becomes more diffused in the vicinity of mean radius and reduces to spherical diffuseness at large distances. The LRA effects corresponding to absorption from a deformed imaginary potential, summed over all orientations, shift to lower energies as compared to undeformed case.

Acknowledgements

The authors are thankful to Drs S S Kapoor, A K Mohanty, M A Nagarajan, D M Nadkarni and A Saxena for many discussions during the course of this work. We acknowledge the fruitful collaboration of Prof. I J Thompson during the course of this work as well as for providing us the FRESCO code.

References

[1] R Vandenbosch, *Annu. Rev. Nucl. Part. Sci.* **42**, 447 (1992)
[2] G R Satchler, *Phys. Rep.* **199**, 147 (1991)
[3] I J Thompson, *Comput. Phys. Rep.* **7**, 167 (1988)
[4] I J Thompson, M A Nagarajan, J A Lilley and M J Smithson, *Nucl. Phys.* **A505**, 84 (1989)
[5] C H Dasso and S Landowne, *Comput. Phys. Comm.* **46**, 187 (1987)
[6] D M Nadkarni, A Saxena, D C Biswas, R K Choudhury, S S Kapoor, N Majumdar and P Bhattacharya, *International Nucl. Phys. Symposium Book of Abstracts* **B85**, (1995)
[7] G R Satchler, M A Nagarajan, J S Lilley and I J Thompson, *Phys. Rev.* **C41**, 1869 (1990)
[8] M Rhoades-Brown and P Braun-Munzinger, *Phys. Lett.* **B136**, 19 (1984)
[9] S V S Sastry, S K Kataria, A K Mohanty and I J Thompson, *Phys. Rev.* **C54**, 3286 (1996)
[10] R A Broglia and A Winther, *Heavy ion reactions* (Addison-Wesley, Redwood City, 1991) p. 463
[11] G R Satchler, M A Nagarajan, J A Lilley and I J Thompson, *Ann. Phys. (N.Y.)* **178**, 110 (1987)
[12] S V S Sastry, A K Mohanty and S K Kataria, *Proceedings of DAE Nucl. Phys. Symposium* **B39**, 132 (1996)